Seismic Evidence for Water Deep in Earth's Upper Mantle

Mark van der Meijde,* Federica Marone, Domenico Giardini, Suzan van der Lee

Water in the deep upper mantle can influence the properties of seismic discontinuities in the mantle transition zone. Observations of converted seismic waves provide evidence of a 20- to 35-kilometer-thick discontinuity near a depth of 410 kilometers, most likely explained by as much as 700 parts per million of water by weight.

Two major seismic velocity discontinuities, at nominal depths of 410 and 660 km, border the transition zone of Earth's mantle. The 410-km discontinuity is the result of the transition from olivine to wadsleyite. The 660-km discontinuity is caused by the transition from ringwoodite to perovskite and magnesiowüstite. Both phase transition intervals are reported to be sharp (about 4 to 10 km thick) (1–3). However, there are conditions under which the transition interval of the 410-km discontinuity can be thickened, such as by an increase in water content in olivine or by a decrease in temperature. Theoretical studies (4, 5) have shown how water influences the properties of the olivine-wadsleyite phase transition. Because water is preferentially incorporated into wadsleyite rather than olivine, it stabilizes wadsleyite over a wider range of pressures and temperatures, thereby thickening the transition interval. This has been confirmed by experiments (6) showing that under hydrous conditions, the zone of coexistence of olivine and wadsleyite can thicken to as much as 40 km. A decrease in temperature would also thicken the transition interval (7), but the effect of temperature on the transition-interval thickness is much smaller than the effect of water. A large temperature reduction of 800 K would thicken the discontinuity by only 10 km (5). Increased water content in the mantle transition zone would have the opposite effect on the thickness of the phase transition interval at 660 km. This phase transition interval would become thinner because ringwoodite can hold much more water than perovskite, thereby extending its stability phase (8). Moreover, recent studies indicate that the phase transition interval from wadsleyite to ringwoodite, nominally at a depth of 520 km, can be sharper under hydrous conditions (9) (<15 km thick) than under anhydrous conditions (10) (~60 km thick). Temperature anoma-

lies in the mantle transition zone would have no seismically observable effect on the thickness of the 660-km discontinuity (7), whereas the effect on the 520-km discontinuity is unknown.

Both temperature and water content of the upper mantle vary spatially. A variety of evidence (11–14) has indicated that amounts of 1500 parts per million (ppm) of water can be present locally in the uppermost mantle. This water is carried there by subducting oceanic plates, which release most of the subducted water at depths shallower than 150 km into the mantle wedge overlying the plate (15). Reports of water being able to reside below this depth are based on high-pressure experiments (16) and seismic tomography (17). It is, however, unknown whether and how much water is transported down to 400 km and below. To investigate whether water resides near the mantle transition zone, we studied the properties of seismic discontinuities beneath the Mediterranean region (Fig. 1). This region has been heavily affected by the subduction of oceanic lithosphere for the past 190 million years. Between 190 and 110

million years ago (Ma), subduction mainly took place in the eastern Mediterranean with mostly south- and eastward-dipping subduction. Remnants of the subducted slab can be found in the lower mantle between 1300 and 1900 km depth under locations such as Egypt and Libya (18). Subduction was ubiquitous after 80 Ma. At present, active subduction zones are found in southern Italy and Greece. We investigated seismic discontinuities in the deep upper mantle of the Mediterranean region by searching seismograms for seismic S waves that converted from P waves at the discontinuities. Our search was facilitated by a recent temporary deployment of mobile broadband seismic stations [MIDSEA (19)] along the plate boundary between Eurasia and Africa. We analyzed over 500 seismograms recorded in the Mediterranean region at 18 temporary and 6 permanent broadband stations (Fig. 1). We identified converted waves by analyzing receiver functions (20).

We found P-to-S converted waves from the 410- and 660-km discontinuity for practically all stations. The conversions from the 410-km discontinuity are small in amplitude for receiver functions that are low-passed with corner frequencies higher than 0.5 Hz. The amplitudes increase with decreasing corner frequency. This effect is not observed for conversions from the 660-km discontinuity, which show comparable amplitudes throughout the whole frequency range.

Because of the temporary deployment of the network and differences in site characteristics, not all seismic stations yielded equally robust results. Receiver functions for nine stations, however, had a sufficiently high signal-to-noise ratio to show unambiguous evidence for this frequency dependence of the P-to-S conversion from the 410-km dis-
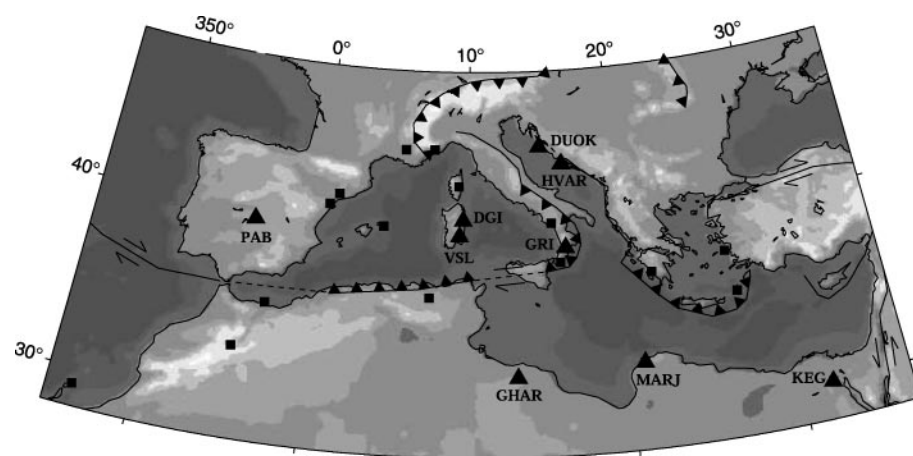
Fig. 1. Map of the Mediterranean region with seismic station and approximate plate boundary locations. Stations for which results are discussed in this paper are represented by black triangles and labeled with the station name (table S1); other analyzed stations are represented by black squares. Curves with a sawtooth pattern indicate the present location of the convergent boundary, with sawteeth pointing in the direction of subduction or underthrusting. Strike-slip is represented by arrows. The gray scale indicates topography ranging from higher than 2.5 km in white to deeper than −2.5 km in dark gray.

Institute of Geophysics, Eidgenössische Technische Hochschule–Hönggerberg (HPP)/Swiss Federal Institute of Technology CH–8093 Zürich, Switzerland.

*To whom correspondence should be addressed. E-mail: mark@tomo.ig.erdw.ethz.ch

continuity (Fig. 2). For the other stations, the receiver functions were more ambiguous and did not allow a significant interpretation of the frequency dependence. For these nine stations, the amplitude of the converted waves from the 410-km discontinuity depends on frequency with 75% confidence, on average, whereas this confidence is only 21% for the 660-km discontinuity (table S2). This indicates that the observed frequency dependence is almost four times more probable for conversions from the 410-km discontinuity than for those from the 660-km discontinuity.

We observed converted energy from the 410-km discontinuity that is significant (20) above the 95% confidence level for corner frequencies around 0.2 and 0.25 Hz for most stations. For station PAB, the amplitude of the wave converted at the 410-km discontinuity becomes comparable to that of the wave converted at the 660-km discontinuity for frequencies as low as 0.15 Hz. This frequency dependence of the amplitudes and the significance allows us to estimate the thickness of the phase transition interval (20).

These findings indicate that the phase transition around 410 km depth is not sharp and occurs over depth intervals of about 20 to 25 km for these stations (fig. S1). For station PAB, however, the transition appears to occur over an interval of about 30 to 35 km. This agrees with an apparent weak contrast found beneath eastern Spain that could not be explained with a first-order discontinuity (21). Such a broad interval could be the reason why previous receiver function studies (22, 23) found no 410-km discontinuity under this station. In agreement with previous ob-

servations (1–3), we found that the phase-transition interval at 660 km is relatively thin (<5 km) beneath seven of the nine stations (Fig. 2, fig. S1, and table S2).

Because of limited azimuthal coverage, owing to the location of the Mediterranean with respect to seismogenic zones, we could not investigate the azimuthal influence on the frequency dependence of the converted waves. However, the conversion points at the 410-km discontinuity beneath most stations fall within a radius of 100 km. Synthetic tests (24) (fig. S3) showed that topography on the discontinuity as large as 20 to 40 km on a 100-km length scale cannot be responsible for the observed frequency dependence. Topography on the 410-km discontinuity would mainly decrease the amplitudes of P-to-S converted waves but could not be responsible for the observed frequency dependence. We also excluded scattering of converted energy from discontinuities at shallower depths as a possible cause for the observed frequency dependence, because the standard deviation of the converted wave from the 410-km discontinuity is comparable to the standard deviation of the converted wave from the 660-km discontinuity. Seismic tomography (25) has shown that large temperature anomalies, which could affect the transition interval thickness, are not expected at these depths beneath the nine stations. The maximum temperature anomaly is estimated to be around 300 K, which would lead to a broadening of less than 10 km (7). Using different velocity models for the depth conversion (both global and local) does not influence the frequency dependence of the converted waves from the

410-km discontinuity. Trace elements in olivine are unlikely to be the cause of the broadening, because their presence would thicken the phase transition interval by no more than 2 km (26).

We interpret the broadening of the 410-km discontinuity deduced here as being caused by water in the mantle minerals at this depth. These minerals can contain a substantial amount of water: as much as 1000 ppm by weight of water in olivine and about 20,000 ppm by weight of water in wadsleyite (27). The estimated water content in olivine for a transition interval of 20 to 25 km is around 500 ppm by weight (Fig. 3). To broaden the transition to 30 to 40 km, olivine would need to contain 700 to 1000 ppm by weight of water. This amount of water is an underestimate because the converted waves are the most sensitive to the lower part of the phase transition interval, where the fraction of wadsleyite increases more rapidly with increasing depth (Fig. 3) and the corresponding gradient in seismic velocity is the steepest.

For some stations (Fig. 2), we also observed, above the 95% confidence level, waves that converted at the 520-km discontinuity. Water would make the corresponding phase transition interval thinner and therefore detectable by high-frequency receiver functions. However, we did not observe a positive correlation between the estimated thickening of the 410-km discontinuity and thinning of the 520-km discontinuity. More seismograms need to be recorded to reduce the large uncertainties for the observed conversions from the 520-km discontinuity, thereby permitting a meaningful estimate of a correlation coefficient. Moreover, the distribution of water in the mantle transition zone does not need to be homogeneous but likely depends strongly on factors such as the configuration and type of past subduction and the composition of the downgoing lithosphere. We also observed splitting of this discontinuity beneath some

Fig. 2. Stacked receiver functions for nine stations in the Mediterranean region processed with different low-pass filters. In each panel, from left to right, corner frequencies of approximately 0.75, 0.62, 0.5, 0.4, 0.35, 0.3, 0.25, 0.2, and 0.15 Hz, respectively, have been used. Assuming a Gaussian distribution, the standard deviation of the stacked receiver functions was calculated, allowing an interpretation of the statistical significance of the converted waves. We define the significance of a converted wave as the gray area between zero amplitude and the lower boundary of the double standard deviation. In other words, we identify waves that have amplitudes larger than zero with 95% confidence.
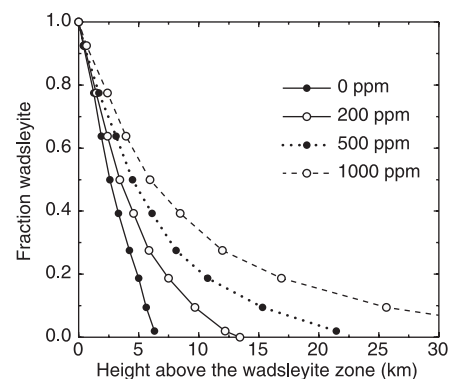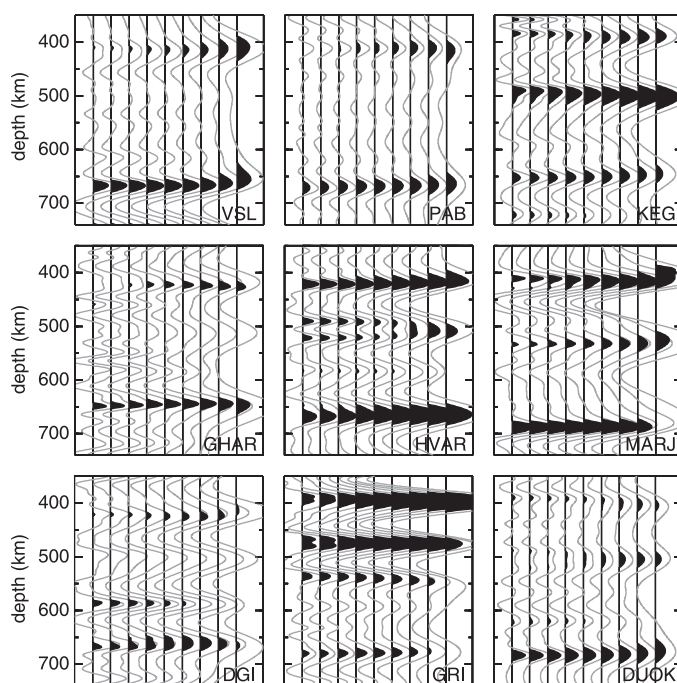
Fig. 3. The olivine-wadsleyite phase transition interval for initial water contents in olivine of 0, 200, 500, and 1000 ppm by weight [after Wood (4)]. For a phase transition thickness of 20 to 25 km, about 500 ppm by weight of water needs to be present.

stations, which has been reported for other subduction zones, especially in southeast Asia (*28*). In addition to previous explanations for this splitting (*28*), we speculate that the split 520-km discontinuity could also be explained by an increased water content in the mantle transition zone.

References and Notes

1. A. Yamazaki, K. Hirahara, *Geophys. Res. Lett.* **21**, 1811 (1994).
2. H. Benz, J. Vidale, *Nature* **365**, 147 (1993).
3. H. Paulssen, *J. Geophys. Res.* **93**, 10489 (1988).
4. B. Wood, *Science* **268**, 74 (1995).
5. G. Helffrich, B. Wood, *Geophys. J. Int.* **126**, F7 (1996).
6. J. Smyth, D. Frost, *Geophys. Res. Lett.* **29**, 10.1029/2001GL014418 (2002).
7. C. Bina, G. Helffrich, *J. Geophys. Res.* **99**, 15853 (1994).
8. Y. Higo, T. Inoue, T. Irifune, H. Yurimoto, *Geophys. Res. Lett.* **28**, 3505 (2001).
9. T. Inoue, D. Weidner, P. Northrup, J. Parise, *Earth Planet. Sci. Lett.* **160**, 107 (1998).
10. M. Akaogi, E. Ito, A. Navrotsky, *J. Geophys. Res.* **94**, 15671 (1989).
11. O. Sigmarsson, M. Condomines, J. Morris, R. Harmon, *Nature* **346**, 163 (1990).
12. P. Ulmer, *Phys. Earth Planet. Inter.* **127**, 215 (2001).
13. S. van der Lee, D. James, P. Silver, *J. Geophys. Res.* **106**, 30821 (2001).
14. The Andean Continental Research Project Working Group, *Nature* **397**, 341 (1999).
15. A. Thompson, *Nature* **358**, 295 (1992).
16. D. J. Frost, Y. Fei, *J. Geophys. Res.* **103**, 7463 (1998).
17. A. Zielhuis, G. Nolet, *Science* **265**, 79 (1994).
18. H. Bijwaard, W. Spakman, E. Engdahl, *J. Geophys. Res.* **103**, 30055 (1998).
19. S. van der Lee *et al.*, *Eos* **82**, 637 (2001).
20. Materials and methods are available as supporting material on *Science* Online.
21. N. A. Pino, D. V. Helmberger, *J. Geophys. Res.* **102**, 2953 (1997).
22. W. Hanka *et al.*, *Eos* **82**, 910 (2001).
23. S. Chevrot, L. Vinnik, J.-P. Montagner, *J. Geophys. Res.* **104**, 20203 (1999).
24. S. van der Lee, H. Paulssen, G. Nolet, *Phys. Earth Planet. Inter.* **86**, 147 (1994).
25. F. Marone, S. van der Lee, D. Giardini, in preparation.
26. G. Gudfinnsson, B. Wood, *Am. Mineral.* **83**, 1037 (1998).
27. D. Kohlstedt, H. Keppler, D. Rubie, *Contrib. Mineral. Petrol.* **123**, 345 (1996).
28. A. Deuss, J. Woodhouse, *Science* **294**, 354 (2001).
29. We thank C. Bina, D. Frost, K. Regenauer-Lieb, G. Helffrich, and H. Paulssen for advice and critical comments on the manuscript. Supported by the Swiss National Science Foundation.

Laboratory Simulation of Charge Exchange–Produced X-ray Emission from Comets

P. Beiersdorfer,[1]* K. R. Boyce,[2] G. V. Brown,[2] H. Chen,[1] S. M. Kahn,[3] R. L. Kelley,[2] M. May,[1] R. E. Olson,[4] F. S. Porter,[2] C. K. Stahle,[2] W. A. Tillotson[2]

In laboratory experiments using the engineering spare microcalorimeter detector from the ASTRO-E satellite mission, we recorded the x-ray emission of highly charged ions of carbon, nitrogen, and oxygen, which simulates charge exchange reactions between heavy ions in the solar wind and neutral gases in cometary comae. The spectra are complex and do not readily match predictions. We developed a charge exchange emission model that successfully reproduces the soft x-ray spectrum of comet Linear C/1999 S4, observed with the Chandra X-ray Observatory.

X-ray emission from comets is localized to a 10^4- to 10^5-km region of the cometary coma between the comet's nucleus and the Sun (*1–5*). The spatial morphology and total luminosity of the emission can be explained by charge exchange between heavy ions in the solar wind and cometary gases (*4–7*). Charge exchange competes with two other explanations considered possible: (i) the scattering of solar x-rays by attogram (10^{-19} g)–sized dust particles and (ii) line and continuum plasma emission heated by turbulence driven by counterstreaming ions (*8, 9*). Cometary x-rays can serve as a diagnostic for solar activity and thus for "space weather" by measuring the quantity and composition of the heavy ion flux in the solar wind. In addition, recent work has shown that the emission is a potential diagnostic of the speed of the solar wind (*10–12*). Because comets enter the solar system from different directions in and out of the ecliptic, they probe regions that are not covered by spacecraft.

We used the spare x-ray microcalorimeter spectrometer (XRS) from the ASTRO-E satellite mission to study charge exchange–induced cometary x-ray emission (*13*). The XRS consists of a 6×6–pixel array with 32 active channels, forming a combined active area of 13 mm^2 operating at 59 mK (*14*). The XRS was designed to view extended objects, such as supernova remnants, with an energy resolution better than 10 eV. This resolution is an order of magnitude better than that available with the Chandra X-ray Observatory or with that of other laboratory instrumentation (*12, 15*).

The XRS was installed at the Lawrence Livermore EBIT-I electron beam ion trap.

The measurements were carried out during the magnetic mode of operation (*16, 17*), in which trapped ions interact with selected gases. The temperature of the ions of interest is about 200 to 300 eV.

The XRS spectrum of helium-like O^{6+} is dominated by the forbidden $1s2s\ ^3S_1 \rightarrow 1s^2\ ^1S_0$ emission, though to a considerably smaller degree than assumed by the most recent predictions (Fig. 1). In contrast, early modeling predictions favored the $1s2p\ ^1P_1 \rightarrow 1s^2\ ^1S_0$ resonance line (*6, 10, 18*), and a more recent prediction favored the $1s2p\ ^3P_1 \rightarrow 1s^2\ ^1S_0$ intercombination line (*11*) in the $n = 2$ emission (fig. S1). The dominance of the forbidden $1s2s\ ^3S_1 \rightarrow 1s^2\ ^1S_0$ line cannot result from collisional excitation but is a signature of charge exchange.

The spectrum of hydrogen-like O^{7+} is very different from that of the helium-like O^{6+} emission (Fig. 2). Unlike the O^{6+}
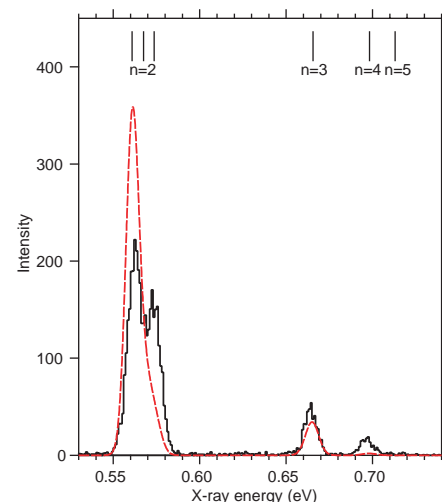
Fig. 1. K-shell emission of O^{6+} produced by charge exchange between O^{7+} and CO_2. Line identifications and energies are given in table S1. The dashed red curve represents a recent radiative cascade model (*23*).

[1]Lawrence Livermore National Laboratory, 7000 East Avenue, L-260, Livermore, CA 94550, USA. [2]NASA/Goddard Space Flight Center, Code 662, Greenbelt, MD 20771, USA. [3]Department of Physics, Columbia University, 538 West 120th Street, New York, NY 10027, USA. [4]University of Missouri–Rolla, Department of Physics, 1870 Miner Circle, Rolla, MO 65409, USA.

*To whom correspondence should be addressed. E-mail: beiersdorfer@llnl.gov